Catalysis Today 147S (2009) S185–S190

Contents lists available at ScienceDirect

Catalysis Today

journal homepage: www.elsevier.com/locate/cattod

Performance of reverse flow monolithic reactor for water–gas shift reaction

Pablo Marín, Salvador Ordóñez *, Fernando V. Díez

Department of Chemical Engineering and Environmental Technology, University of Oviedo, Facultad de Química, Julián Clavería 8, Oviedo 33006, Spain

ARTICLE INFO

Article history:
Available online 3 August 2009

Keywords:
Unsteady-state reactors
Structured catalyst
Hydrogen production
Reactor modeling

ABSTRACT

This work explores the application of monolithic catalysts and reverse flow reactor (RFR) technology for carrying out the water–gas shift reaction (WGS). The performance of both adiabatic fixed-bed reactors (FBR) and RFR operating with particulate or monolith catalysts has been simulated using a heterogeneous one-dimensional model, experimentally validated for other reactions in previous works. Comparisons were made at the same space velocities (*GHSV* between 6000 and 12000 h^{-1}) and at previously optimized values of switching time (RFR) and feed temperature (FBR).

Results obtained indicate that the operation with monolith catalysts provide better results in terms of wider stability intervals (RFR) and hydrogen yields (both RFR and FBR). When the performances of FBR and RFR are compared, it is observed that, for the same amount of catalyst, the FBR performs better than the FBR, although the difference becomes smaller as the space time increases. So, for high space times, the use of monolithic RFR can be advantageous taking into account the higher energy efficiency of RFR, which may allow operation with no feed heating.

1. Introduction

In the last years, the development of the hydrogen economy has increased the research on hydrogen production technologies. Among these technologies, the water–gas shift reaction (WGS) plays a key role in the synthesis of hydrogen from different raw materials (natural gas, biogas, oil fractions, coal, biomass, etc.). According to this strategy, the organic raw material is transformed, through gasification or reforming, into a mixture of hydrogen and carbon monoxide (syngas). Carbon monoxide is a poison for polymer electrolyte membranes fuel cells, so its concentration must be reduced to less than 50 ppm [1,2]. By means of the WGS reaction, carbon monoxide reacts with steam to produce carbon dioxide and hydrogen, thus increasing the hydrogen yield. The remaining carbon monoxide is usually eliminated by catalytic preferential oxidation. Finally, carbon dioxide can be easily separated from hydrogen (if necessary) by gas absorption or pressure swing adsorption [3–5].

The WGS reaction is exothermic ($\Delta H_R = -41.2$ kJ/mol) and strongly equilibrium-limited ($K_{eq} = \exp(4577.8/T - 4.33)$). So, in order to achieve high conversions, the commercial process uses a multi-stage catalytic fixed-bed reactor (FBR) with inter-stage cooling, and an excess of steam. Normally, two catalytic beds are used, the first one operating at high temperature (350–600 °C) with a Fe_3O_4–Cr_2O_3 catalyst, and the second one operating at low temperature (150–250 °C) with a CuO/ZnO catalyst [2,4]. However, this reaction is very slow, so the catalytic beds are very large, resulting in high pressure drops. Although WGS equilibrium is not affected by pressure, undesired secondary reactions, such as methanation, are favored at high pressures. Therefore, monolithic beds present important advantages for this reaction, as they produce substantially lower pressure drops than traditional particulated beds. The interest of monoliths for the WGS reaction has increased, as they can be used as integrated reforming processes to produce hydrogen for small-scale applications, such as in the automotive industry. Moreover, monolithic beds are also desired in these situations, due to the improved mechanical robustness of the reactor, necessary for on board applications [1,2].

Reverse flow reactors (RFR) belong to an important group of catalytic reactors operating under forced unsteady-state conditions, where the unsteady-state is achieved by periodically reversing the feed flow direction. The main advantages of this operation are improved concentration and temperature profiles that lead to higher conversions for certain reactions, and the possibility of constructing integrated devices where reaction and heat exchange or separation take place simultaneously [6–9]. When working with exothermic reactions and low temperature feeds the temperature profiles in the reactor are characteristically parabolic, with lower temperature at the reactor ends and higher temperature in the centre. These temperature profiles are advantageous for reversible reactions, such as the WGS reaction considered in this work, because the high temperature of the reactor centre increases the reaction rate, approaching the equilibrium faster, and the low temperature of the reactor ends

* Corresponding author. Tel.: +34 985 103 437; fax: +34 985 103 434.
E-mail address: sordonez@uniovi.es (S. Ordóñez).

0920-5861/$ – see front matter © 2009 Elsevier B.V. All rights reserved.
doi:10.1016/j.cattod.2009.07.004

shifts the equilibrium. The performance of the RFR for carrying out the WGS reaction has not been studied previously, though satisfactory results have been obtained for another important reversible reaction, i.e. the oxidation of sulfur dioxide to sulfur trioxide [7,10]. In addition, RFR have also been considered for other steps of the hydrogen production process, namely the autothermal catalytic steam reforming [11,12], and partial oxidation of methane [13]. In previous works, we have explored the application of RFR to the catalytic combustion of methane and VOC air lean mixtures and the selective catalytic reduction of NO_x [6,8,14]. For more information about the applications of RFR see the reviews published by different authors [7,11,15].

The scope of this work is to explore the application of a monolithic RFR to the WGS reaction, as part of an integrated low-scale hydrogen production process. A model Fe–Cr catalyst has been considered for this purpose, and the performance of monolithic and conventional particulated catalysts has been compared. Moreover, the performance of RFR has been compared with a conventional FBR, for both types of beds, monolithic and particulated. The study has been carried out by means of simulations from a 1D heterogeneous dynamic model in adiabatic conditions. Typical industrial operating conditions are considered in the simulations. Due to the importance of the space velocity (expressed as *GHSV*), in comparison with the other operating conditions, different *GHSV* values have been considered in the range of typical industrial operation, 6000–12000 h^{-1} (measured at 1 bar and 25 °C) [2,16]. Other important operational variables, such as the switching time for the RFR and the inlet temperature for the FBR, have been varied and selected in order to achieve higher CO conversions.

2. Mathematical modeling

The RFR simulations were performed considering a heterogeneous 1D dynamic model, derived from conservation equations applied separately to the gas and solid phases. For the case of the monolith bed, the same behavior for all the channels (that represent the entire bed) has been assumed. The reactor is considered to be adiabatic (there is no heat transfer between the reactor wall and the surroundings), which is a very good approximation for big industrial reactors with large diameter. This model has been used and experimentally validated in the literature for simulating the behavior of monolith and particulate beds, both considered in this work [6,14,17]. The following set of partial differential equations is obtained after simplifying the conservation equations, taking into account that total molar flow does not change during the water–gas shift reaction. In addition, the following considerations have been taken into account:

- Ideal gas behavior is assumed for the gas phase.
- Non-ideal flow is considered using dispersion terms in the mass and energy balances [1].
- Mass and heat transfer between the solid and gas phases is modelled by means of the proper transport coefficients [1,18].
- Mass transfer inside the catalyst particle and the washcoat layer of the monolith is modelled with the introduction of an effectiveness factor [14,19].

Mass balance to the gas phase:

$$\frac{\partial y_{Gj}}{\partial t} = v_0 \frac{\rho_{Go}}{\rho_G} \frac{\partial y_{Gj}}{\partial z} + D_{j,ax} \frac{\partial^2 y_{Gj}}{\partial^2 z} - a_G K_{Gj}(y_{Gi} - y_{Si}) \quad (1)$$

Mass balance to the solid phase:

$$\frac{\partial y_{Sj}}{\partial t} = a_S K_{Gj}(y_{Gi} - y_{Si}) + \frac{\eta_j \rho_{cat} f_w (r_j)_m}{c_G} \quad (2)$$

Energy balance to the gas phase:

$$\frac{\partial T_G}{\partial t} = -v_0 \frac{\rho_{Go}}{\rho_G} \frac{\partial T_G}{\partial z} + \frac{\kappa_{G,ax}}{\rho_G C_{PG}} \frac{\partial^2 T_G}{\partial z^2} + \frac{a_G h}{\rho_G C_{PG}} (T_S - T_G) \quad (3)$$

Energy balance to the solid phase:

$$\frac{\partial T_S}{\partial t} = \frac{\kappa_{S,ax}}{\rho_S C_{PS}} \frac{\partial^2 T_S}{\partial z^2} + \frac{a_S h}{\rho_S C_{PS}} (T_G - T_S) + \frac{\sum_{j=1}^{C} \eta_j \rho_{cat} f_w (r_j)_m \Delta H_j}{\rho_S C_{PS}} \quad (4)$$

Transport and dispersion parameters of the previous equations are calculated using different correlations for particulate and monolithic beds from the literature, as summarized in Table 1. The kinetic expression obtained by Keiski et al. [20] for the WGS reaction over a commercial Fe_3O_4–Cr_2O_3 catalyst has been adopted, as described by the following expressions:

$$(r_j)_m = -k_m (c_{CO})^{0.72} (c_{H_2O})^{0.10} (1 - \beta), \quad \text{with } \beta = \frac{c_{CO_2} c_{H_2}}{c_{CO} c_{H_2O} K_{eq}} \quad (5)$$

$$k_m = 2.05 \times 10^3 \exp\left(-\frac{7861}{T_s}\right) \quad (6)$$

The kinetic parameters in Eqs. (5) and (6) are intrinsic, obtained in the absence of transport resistances. As a result, appropriate effectiveness factors for the particulated or monolithic catalyst must be used (Table 1). The linearization method of Lommerts et al. [19] has been shown to be a good estimation method for this reaction. First, the kinetic equation is approximated to reversible first order, which is used to calculate the Thiele modulus and then the effectiveness factor. The effectiveness factor values calculated this way are within the range of typical values found in the literature [21]. The approximate kinetic equation is only used in the calculation of the effectiveness factor; in the balance equations the full equation proposed by Keiski et al. is used.

The previous set of partial differential equations is solved considering Danckwerts boundary conditions, using the 'method of lines'. According to this method, first, the spatial derivatives are approximated using finite differences in a grid along the axial coordinate (a gird of 100 points has been used with satisfactory results), and then the resulting set of ordinary differential-algebraic equations is solved using an appropriate algorithm for stiff problems. The effect of changing the flow direction in the RFR is simulated by shifting the axial coordinate at the end of every half-cycle during the resolution of the model. The model has been solved with a MATLAB code using the function *ode15s*. This method has been shown to be adequate for simulating this type of reactors in previous works [6,14].

3. Results and discussion

The scope of the first set of simulations was to show that the WGS reaction can be successfully carried out in a RFR using a monolithic catalyst bed. In Fig. 1, pseudo-steady state conversion and temperature profiles along the reactor at the beginning, middle and end of a direct half-cycle (from left to right) are shown. The simulations were performed using the parameters listed in Tables 2 and 3, which correspond to typical particulated and monolithic catalyst [1,20], together with a space velocity (*GHSV*) of 9000 h^{-1} and a switching time of 100 s. The reactor feed concentration is the corresponding to a reformate syngas [2,16]. As shown in Fig. 1, conversion and temperature profiles move during the half-cycle in the direction of the flow, due to the entrance of cold gas. The RFR exhibits a characteristic parabolic temperature profile with a temperature maximum situated in the centre of the bed of around 600 °C (it should be noted that this temperature is within the operation interval of the high-temperature WGS catalysts), and temperature decreasing in both

Table 1
Equations used for the calculation of the transport and geometric properties of the particulated and monolithic beds.

Particulated bed

Geometry:
$a_G = \frac{6}{d_p}\left(\frac{1-\varepsilon}{\varepsilon}\right), \quad a_S = \frac{6}{d_p}$

Gas–solid transport [18]:
$Nu = 2 + f(Re, Pr)Re^{1/2}Pr^{1/3}$
$Sh_j = 2 = f(Re, Sc)Re^{1/2}Sc_j^{1/3}$

Axial dispersion [18]:

$D_{j,ax} = \left(\frac{d_p \upsilon_0 \rho_{G0}}{\rho_G}\right)\left[\frac{0.73}{ReSc_j} + \frac{0.5}{1+(9.7/ReSc_j)}\right]$

$\kappa_{G,ax} = d_p \upsilon_0 \rho_{G0} C_{PG}\left[\frac{0.73}{RePr} + \frac{0.5}{1+(9.7/RePr)}\right]$

$k_{S,ax} = k_G\left[\left(\frac{2\sqrt{1-\varepsilon}}{f_n}\right)\right]\left[\frac{f_e}{f_n^2}\left(1-\frac{k_G}{k_S}\right)\log\left(\frac{k_S}{f_e k_G}\right) - \frac{b+1}{2} - \frac{b-1}{f_n}\right] + (1-\sqrt{1-\varepsilon})\left(1+\frac{K_R}{K_G}\right) + \frac{\sqrt{1-\varepsilon}}{(\kappa_G/\kappa_R)+(\kappa_G/\kappa_S)}$

Internal effectiveness factor [14]:
$\eta_j = \frac{3}{\phi_j}\left(\frac{1}{\tanh\phi_j} - \frac{1}{\phi_j}\right)$

Monolithic bed

Geometry:
$a_G = \frac{4}{D_h}, \quad a_S = \frac{4}{D_h}\left(\frac{\varepsilon}{1-\varepsilon}\right)$

Gas–solid transport [1]:

$Nu = \frac{Nu_H}{2} - \frac{Da}{2}\frac{Nu_H}{Nu_T} + \frac{1}{2}\sqrt{\left(Nu_H - Da\frac{Nu_H}{Nu_T}\right)^2 + 4DaNu_H}$

$Nu_H = 3.095 + 8.933\left(\frac{1000}{l^*}\right)^{-0.5386}\exp\left(-\frac{6.7275}{l^*}\right)$

$Nu_T = 2.977 + 6.854\left(\frac{1000}{l^*}\right)^{-0.5174}\exp\left(-\frac{42.49}{l^*}\right)$

$Sh_j = \frac{Sh_{H,j}}{2} - \frac{Da_j}{2}\frac{Sh_{H,j}}{Sh_{T,j}} + \frac{1}{2}\sqrt{\left(Sh_{H,j} - Da_j\frac{Sh_{H,j}}{Sh_{T,j}}\right)^2 + 4Da_j Sh_{H,j}}$

$Sh_{H,j} = 3.095 + 8.933\left(\frac{1000}{l^*}\right)^{-0.5386}\exp\left(-\frac{6.7275}{l_j^*}\right)$

$Sh_{T,j} = 2.977 + 6.854\left(\frac{1000}{l^*}\right)^{-0.5174}\exp\left(-\frac{42.49}{l^*}\right)$

Axial dispersion [1]:

$D_{j,ax} = D_{jm} + \frac{(\upsilon D_h)^2}{192 D_{jm}}$

$\kappa_{G,ax} = \kappa_G + \frac{(\upsilon D_h \rho_G C_{PG})^2}{192\kappa_G}$
$\kappa_{S,ax} = \kappa_S$

Internal effectiveness factor [14]:
$\eta_j = \frac{\tanh\phi_j}{\phi_j}$

reactor ends down to the inlet gas temperature (25 °C). This shows that the syngas enters the reactor at low temperature and is pre-heated using the heat stored in the bed during the previous cycle, while, simultaneously more heat is released by the reaction. The reaction proceeds with high reaction rate, until the equilibrium is reached at the centre of the reactor (in the zone of maximum temperature). As the reactants circulate towards the reactor exit, temperature decreases. This decrease shifts the equilibrium towards formation of products, hence producing higher conversions. This effect is observed by the change in the slope of the CO conversion profiles. This parabolic temperature profile is much more efficient for reversible reactions than the typical increasing temperature profiles of FBR, higher conversions being obtained at the reactor exit [7,10].

Once demonstrated that the WGS reaction can be carried out in a RFR, the performance of the reactor using particulated and monolithic beds was compared. The comparison has been done in terms of the CO outlet conversion and the maximum solid

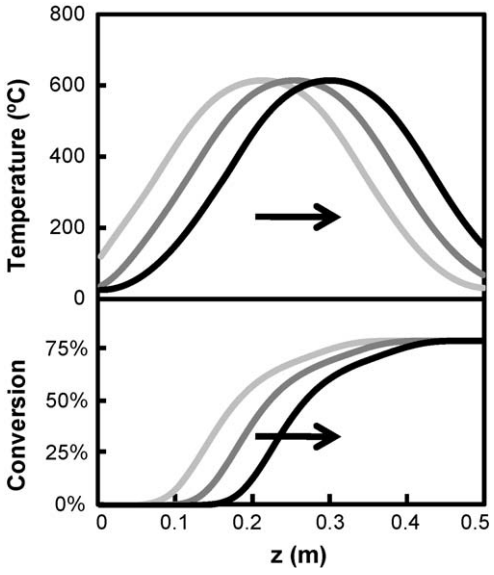

Fig. 1. Solid temperature and CO conversion profiles for a monolithic RFR. *GHSV* = 9000 h^{-1}, t_{sw} = 100 s. Beginning (▭), middle (▭), and end (▬) of cycle. Flow direction is indicated by an arrow.

temperature, as shown in Fig. 2. The curves depicted in Fig. 2 have been obtained by varying the switching time from very low (30 s) to high values (600 s), and for three space velocities (*GHSV* 6000, 9000 and 12000 h^{-1}). Each point corresponds to a different simulation of the RFR up to the pseudo-steady state. The CO conversion curves (Fig. 2a and c) show that stable operation of the RFR with low temperature feeding (25 °C) is only possible for switching times below a characteristic value, called here critical switching time ($t_{sw,cr}$). This happens because, for high witching

Table 2
Geometric and physical properties of the particulated and monolithic beds.

Bed type	Particulated	Monolith
Particle diameter, d_p (m)	3×10^{-3}	–
Hydraulic diameter, D_h (m)	–	10^{-3}
Cell density (cpsi)	–	300
Washcoat layer (m)	–	9×10^{-5}
Bed porosity, ε	0.4	0.54
Washcoat fraction, f_w	1	0.42
Density, ρ (kg/m^3)	1945	2100
Heat capacity, C_p (J/(kg K))	800	900
Thermal conductivity, κ (W/(m K))	0.34	1.5

Table 3
Operating conditions used in the simulations of the RFR and FBR.

Operating conditions	
Reactor length, L_R (m)	0.5
Space velocity @ 25 °C, GHSV (h^{-1})	6000/9000/12000
RFR inlet temperature, T_0 (°C)	25
RFR pre-heating temperature (°C)	400
RFR switching time, t_{sw} (s)	10–600
FB inlet temperature, T_0 (°C)	300–600
Inlet pressure (bar)	1
CO inlet molar fraction	0.06
H_2O inlet molar fraction	0.56
CO_2 inlet molar fraction	0.04
H_2 inlet molar fraction	0.18
N_2 inlet molar fraction	0.16
Catalyst internal properties	
Internal porosity, ε_{pors}	0.5
Internal tortosuity, τ_{pors}	4
Mean pore diameter, d_{pors} (m)	10^{-8}

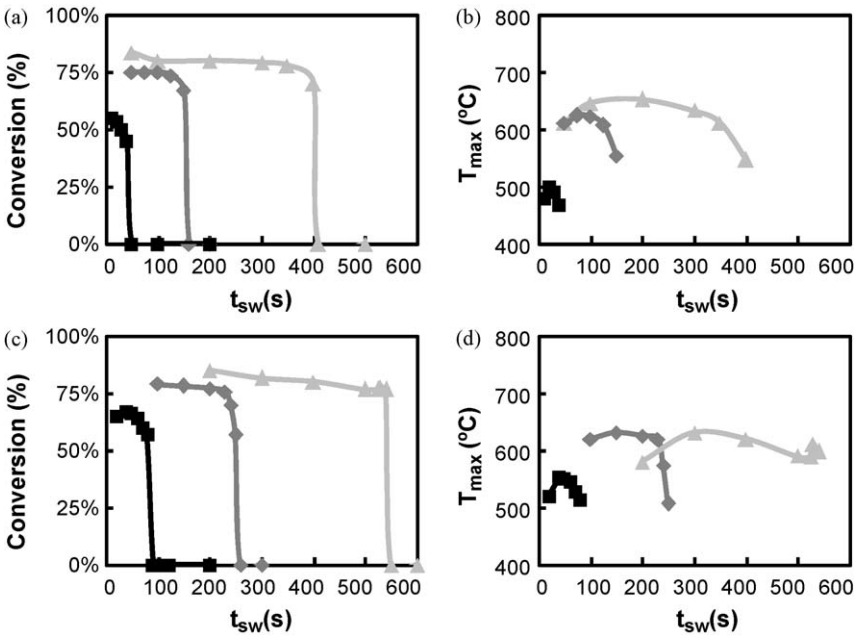

Fig. 2. Stability curves for the RFR. Particulated bed: (a) CO conversion and (b) maximum solid temperature. Monolithic bed: (c) CO conversion and (d) maximum solid temperature. *GHSV* = 6000 h^{-1} (▬), 9000 h^{-1} (▬) and 12000 h^{-1} (▬).

times values, the amount of heat stored inside the reactor between cycles is not enough for pre-heating the feed to the ignition temperature during the whole half-cycle, so that reaction extinction takes place. The value of the critical switching time depends on the physical properties and the operating conditions of the reactor, and it must be determined for each situation either experimentally or by means of simulations. The *GHSV* affects markedly the RFR stability (and hence the critical switching time), as shown in Fig. 2. On increasing the *GHSV*, the reactor becomes less stable, stable operation being only possible for low switching times. High *GHSV* correspond to high gas flow velocities, which makes the temperature profile to move quicker towards the reactor exit, and flow direction must be inverted soon, in order to prevent the high temperature plateau from leaving the reactor.

Comparison between particulated and monolithic RFR (Fig. 2a and c), shows that the monolithic bed is better in terms of reactor stability (its critical switching times are higher for the same operating conditions). Fig. 3a shows the same trend, i.e. the curve of switching time as a function of *GHSV* is always higher for the monolithic bed.

It is interesting to point out that other reactions, such as the catalytic combustion of methane–air lean mixtures, studied in a previous work [14], present the opposite behavior. This is explained by the different nature of both reactions, in terms of kinetics and RFR behavior. The catalytic combustion of methane is a fast irreversible reaction that takes place in a short length of bed, where the reaction heat is released. As a result, the capacity for heat storage of the bed (given by the bed porosity, density, heat capacity and thermal conductivity) determines the thermal behavior of the RFR, which is responsible of its stability. For this reason, RFR with monolith bed, that present higher bed porosity, are less stable for this reaction. In contrast, the WGS reaction is exothermic and reversible, highly affected by mass transport phenomena, particularly internal mass transfer. That is why industrial-scale reactors use small catalyst particles, which, on the other hand, leads to high pressure drops. As shown, monolithic beds perform better than particulated beds for the WGS reaction, regardless of the lower bed porosity, because the catalyst is deposited in the thin washcoating layer of the channel walls. This reduces the mass transfer resistances considerably, for the same operating conditions, resulting in a higher apparent reaction rate. As a result, for the WGS reaction, the poorer capacity for heat storage of the monolith bed is overcome by the higher apparent reaction rate, resulting in a higher RFR stability.

The maximum solid temperature (Fig. 2b and d) also shows the stability differences between particulated and monolithic RFR. Increasing *GHSV* produces a reduction of the maximum temperature, explained by the lower amount of heat stored inside the reactor between cycles.

In the second part of the study, the performances of RFR and conventional FBR reactors for the WGS reaction have been compared. For this purpose, the behavior of the FBR with both particulated and monolithic beds has been determined under different operating conditions. The main results are presented in Fig. 3c and d. Outlet CO conversion at the steady state is depicted as a function of the inlet gas temperature for the same *GHSV* values studied previously for the RFR. In this case, operation with cold feed is impossible, and the feed must be pre-heated before fed to the reactor. Then, inlet gas temperature turns into an important operating variable for FBR, and was varied in this study, in order to determine the best operating conditions. It can be noticed that, for both types of beds (particulated and monolithic), there is an optimum inlet gas temperature that leads to a maximum CO conversion. This behavior is typical from exothermic equilibrium-limited reversible reactions, such as WGS. On increasing the *GHSV*, the maximum moves to higher inlet gas temperatures, but also the value of the maximum conversion decreases slightly. This trend is observed for both beds, particulated and monolithic, although the monolithic bed exhibits slightly higher maximum conversions. This is explained by the better performance of monolithic beds in terms of internal mass transport (higher effectiveness factors), which results in higher apparent reaction rates, as explained before for the RFR.

Finally, RFR and FBR are compared for the monolithic and particulated beds. This comparison is performed in terms of the maximum CO outlet conversion that can be achieved in the different reactors. Thus, using the information reported in Fig. 3c and d, the inlet gas temperatures determining maxima CO outlet

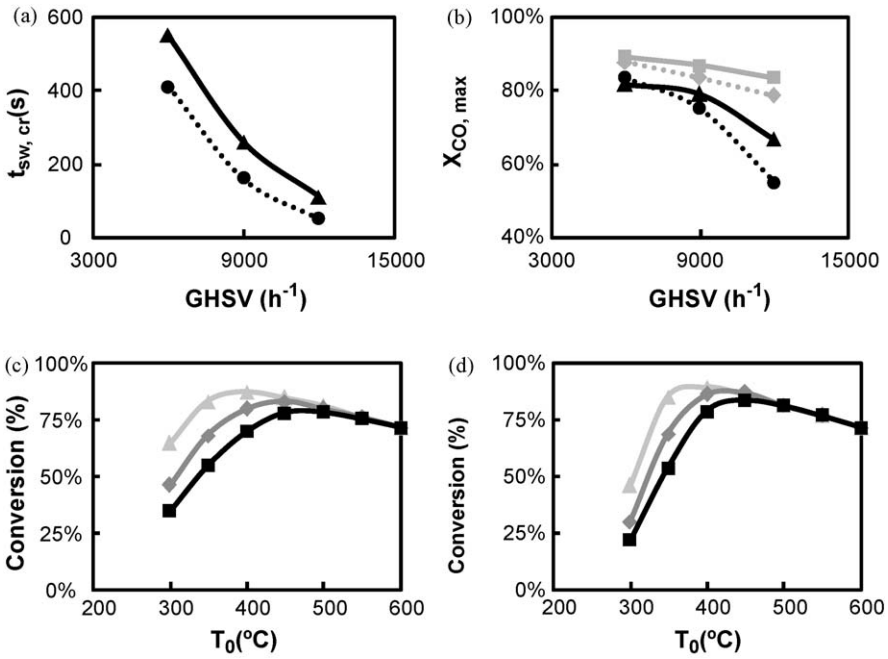

Fig. 3. (a) Influence of the *GHSV* on the critical switching time for the RFR: monolithic (▬) and particulated (•••) beds. (b) Influence of the *GHSV* on the maximum CO conversion. (▬) Monolithic RFR, (•••) particulated RFR, (▬) monolithic FBR, (•••) particulated FBR. (c) and (d) Influence of the inlet gas temperature on the CO conversion for the particulated (c) and monolithic (d) FBR. *GHSV* = 6000 h^{-1} (▬), 9000 h^{-1} (▬) and 12000 h^{-1} (▬).

conversion are identified and selected for comparison. In a similar way, the switching time values corresponding to a maxima CO outlet conversion are obtained from Fig. 2. The results for the different reactors are summarized in Fig. 3b as a function of *GHSV*. As shown, the FBR presents higher maximum CO conversions than the RFR for all the *GHSV* values considered in the study. This effect is explained considering that for the case of the RFR, the temperature in a part of both reactor ends is too low for the reaction to take place in measurable extent, so the catalyst placed at these zones is only being used as a thermal regenerator. As a result, the catalyst of these zones could be substituted by an inert material, in such a way that the RFR we are considering could contain less catalyst than the amount considered. Then, if the comparison between FBR and RFR is done for the same amount of catalyst (and not total solid bed), the comparison would be more favorable for the RFR, in terms of CO conversion.

Moreover, RFR present advantages when compared to the FBR in terms of energy efficiency, due to the RFR high heat integration capacity, which makes possible the operation with low temperature feeding. This way, in the case studied, RFR could energy saving up to 450 kJ/kg, which is the energy required to pre-heat the feed in the FBR. For the case of high temperature feeds, the high RFR heat integration capacity can also be useful. Thus, the hot syngas could be used to pre-heat the feed to the reforming unit, before entering the RFR (as it can work with cold feed). Therefore, the thermal efficiency of the whole process would improve.

Regarding the type of bed, Fig. 3b shows that the monolithic bed always performs better than the particulate bed for both FBR and RFR.

4. Conclusions

RFR are dynamic reactors operating under forced unsteady-state conditions, which can present important advantages for reversible reactions, such as the WGS reaction considered in this work. Moreover, the use of monolithic beds, very common in the environmental industry, is expanding to the chemical industry. In this work, it has been found by means of simulations that for the WGS reaction, monolith beds perform better than particulated beds, for the same operating conditions, for both FBR and RFR. This is explained by the higher apparent reaction rate (higher effectiveness factors) encountered in monolithic beds, due to the intensification of the process. The performance of RFR and FBR has also been compared, resulting in higher CO conversions when operating with the FBR. However, it has been pointed out that substituting the catalyst of the reactor ends by inert material can improved considerably the performance of the RFR. Moreover, the RFR also presents advantages due to the potential energy savings derived from its ability of operating with low temperature feed.

Acknowledgement

This work was financed by the Spanish Ministry for Science and Innovation (contract CIT-120000-2008-4, Applied Collaborative Research Program 2008).

References

[1] A.S. Quiney, G. Germani, Y. Schuurman, Journal of Power Sources 160 (2006) 1163.
[2] W. Ruettinger, O. Ilinich, R.J. Farrauto, Journal of Power Sources 118 (2003) 61.
[3] W.-H. Chen, M.-R. Lin, T.L. Jiang, M.-H. Chen, International Journal of Hydrogen Energy 33 (2008) 6644.
[4] A.B. Mhadeshwar, D.G. Vlachos, Catalysis Today 105 (2005) 162.
[5] O.L. Ding, S.H. Chan, International Journal of Hydrogen Energy 33 (2008) 4325.
[6] P. Marin, S. Ordonez, F.V. Diez, Chemical Engineering Science 63 (2008) 5003.
[7] Y.S. Matros, G.A. Bunimovich, Catalysis Reviews 38 (1996) 1.
[8] P. Marín, D. Fissore, A.A. Barresi, S. Ordóñez, Chemical Engineering and Processing: Process Intensification 48 (2009) 311.
[9] G. Eigenberger, G. Kolios, U. Nieken, Chemical Engineering Science 62 (2007) 4825.
[10] W.-D. Xiao, H. Wang, W.-K. Yuan, Chemical Engineering Science 54 (1999) 4645.
[11] G. Kolios, A. Gritsch, A. Morillo, U. Tuttlies, J. Bernnat, F. Opferkuch, G. Eigenberger, Applied Catalysis B: Environmental 70 (2007) 16.
[12] B. Glockler, G. Kolios, G. Eigenberger, Chemical Engineering Science 58 (2003) 593.
[13] J. Smit, M.V. Annaland, J.A.M. Kuipers, Chemical Engineering Research & Design 82 (2004) 245.

[14] P. Marin, M.A.G. Hevia, S. Ordonez, F.V. Diez, Catalysis Today 105 (2005) 701.
[15] A.A. Barresi, G. Baldi, D. Fissore, Industrial & Engineering Chemistry Research 46 (2007) 8693.
[16] J. Pasel, P. Cremer, B. Wegner, R. Peters, D. Stolten, Journal of Power Sources 126 (2004) 112.
[17] J. Chen, H. Yang, N. Wang, Z. Ring, T. Dabros, Applied Catalysis A: General 345 (2008) 1.
[18] D. Fissore, A.A. Barresi, G. Baldi, M.A.G. Hevia, S. Ordóñez, F.V. Díez, AIChE Journal 51 (2005) 1654.
[19] B.J. Lommerts, G.H. Graaf, A.A.C.M. Beenackers, Chemical Engineering Science 55 (2000) 5589.
[20] R.L. Keiski, O. Desponds, Y.F. Chang, G.A. Somorjai, Applied Catalysis A: General 101 (1993) 317.
[21] S. Lim, J. Bae, K. Kim, International Journal of Hydrogen Energy 34 (2009) 870.